scientific reports

OPEN

High-temperature resistant resonant cavity microwave sensor for precision blade tip clearance monitoring in aeroengines

Haolin Sun[1,2] ✉

In the aerospace field, accurate measurement of the blade tip clearance of aeroengines is highly important for enhancing engine performance and ensuring flight safety. Existing measurement techniques, such as capacitive, inductive, and optical methods, have limitations in terms of stability, application range, or tolerance to complex environments. Moreover, the problem of sensor performance degradation in high-temperature environments has not been effectively resolved. This study aims to design a high-temperature resistant microwave blade tip clearance sensor to overcome these limitations. The sensor structure is designed on the basis of the resonant cavity principle and electromagnetic field theory. The sensor has a radiation efficiency of 97% near 24 GHz, a reflection coefficient as low as 0.01, good measurement resolution within the 0–6 mm clearance measurement range, and the impact of changes in the dielectric constant at high temperatures on its performance is controllable. This research provides a new solution for the measurement of aeroengine blade tip clearance, improving the stability and reliability of the measurement.

As the "heart" of an aircraft, an aeroengine's performance directly affects the aircraft's thrust, fuel efficiency, and safety. During engine operation, the radial clearance (i.e., blade tip clearance) between the high-pressure turbine and compressor blades and the casing is one of the key parameters affecting the engine's overall efficiency[1–3]. When the blade tip clearance is within the ideal range, the engine's thermal efficiency can be significantly improved, reducing the energy loss caused by gas leakage and thereby enhancing the thrust[4,5]. Conversely, excessively large or small blade tip clearances can lead to a series of problems. An overly large blade tip clearance increases gas leakage, reducing the engine's performance and increasing the operating cost. An overly small blade tip clearance may cause friction and collision between the blades and the casing during high-speed rotation, seriously threatening flight safety, accelerating component wear, and shortening the engine's service life[6–8]. Therefore, achieving high-precision real-time monitoring of blade tip clearance has become a crucial requirement for the development of aeroengine technology.

Although blade tip clearance measurement technology has been developed for many years, existing solutions face severe challenges under the extreme operating conditions of aeroengines. Capacitive sensors are vulnerable to interference from humidity and oil, which results in poor measurement stability[9]. Inductive technologies rely on the electromagnetic properties of the material being measured, which limits their versatility. Optical sensors, despite their relatively high accuracy, experience a sharp decline in reliability in the complex environment of the engine interior, which is characterized by high temperatures (> 800 °C), high pressures, oil mists, and vibrations, because the optical path is easily contaminated or blocked[10,11]. In addition, the high-temperature environment imposes extremely high demands on the thermal stability of sensor materials. Traditional sensors often fail because of material softening, dielectric constant drift, or thermal expansion mismatch, and existing research still lacks a systematic solution for compensating for the changes in material properties at high temperatures[12–14]. In gas turbines, blade tips rotate at velocities of 350–450 m/s, with each blade tip exposed to the sensor for only microseconds. This high-speed motion introduces unique challenges, such as the Doppler effect and transient signal acquisition, which must be addressed for accurate clearance monitoring. These limitations make it difficult

[1]Beijing Institute of Technology School of Mechatronical Engineering, Beijing 100081, China. [2]Changcheng Institute of Metrology & Measurement (CIMM), Beijing 100095, China. ✉email: sunhaolin24@163.com

for existing technologies to meet the long-term and high-reliability monitoring requirements of aeroengines, creating a bottleneck restricting engine technology upgrades.

To address the issues mentioned above, this study proposes a high-temperature resistant microwave blade tip clearance sensor based on the resonant cavity principle, with the aim of overcoming the measurement bottleneck in high-temperature environments. Its innovative contributions are reflected in three main aspects. First, the combination of the microwave phase method and the resonant cavity structure enables noncontact, high-precision measurements by analyzing the phase difference of the reflected signal, effectively overcoming the environmental sensitivity of optical and capacitive technologies. Second, through the collaborative design of multiple materials (such as silicon nitride ceramic windows, nickel-based alloy GH4169 casings, and high-temperature resistant coaxial cables), the structural stability and signal fidelity of the sensor in a 1000 °C environment are significantly enhanced. Third, a dynamic compensation model for the high-temperature dielectric constant is established to quantify the impact of material property changes on measurement errors, providing a theoretical basis for the performance optimization of high-temperature sensors. This research not only fills the application gap of existing technologies under extreme operating conditions but also provides new ideas for the clearance monitoring of high-temperature industrial scenarios such as gas turbines and nuclear power equipment, and it possesses important academic value and engineering significance.

Design of the microwave sensor probe with a resonant cavity structure
Measurement principle of the microwave sensor
The microwave sensor testing system measures the blade tip clearance on the basis of the principle of the microwave phase method. The testing principle is as follows: the microwave sensor emits a continuous microwave signal. When a rotating blade passes through the sensor port, the microwave signal is reflected. This reflected signal is then compared with the internal reference signal, generating a phase difference[15,16]. As the blade tip clearance changes, the phase difference changes accordingly. The real-time change value of the blade tip clearance can be obtained on the basis of the change value of this phase difference. Moreover, invalid clearance signals can be removed according to the amplitude value of the echo signal.

Figure 1 shows a schematic diagram of the microwave sensor measurement principle. Assume that the distance between the microwave transmitter and the target is R. Then, in the two-way path of the microwave reaching the target and returning to the sensor, the total number of wavelengths passed is $2R/\lambda$, and the total phase φ change in the two-way propagation path is shown by Eq. (1):

$$\phi = 2\pi \cdot \frac{2R}{\lambda} = \frac{4\pi R}{\lambda} \quad . \tag{1}$$

Assuming that the initial phase of the reference signal emitted by the probe is φ_0, the phase difference between the echo signal and the reference signal is as follows:

$$\phi = \phi_0 + \frac{2R}{\lambda} \cdot 2\pi \quad . \tag{2}$$

In the blade tip clearance measurement, the test displacement is less than the transmission wavelength. To avoid the influence of phase ambiguity, the length of the two-way path of the signal must be within one wavelength of the microwave operating frequency; that is, the test distance must be less than half of the wavelength range $(2R/\lambda < 1)$.. From Eq. (2), the calculation equation for the clearance distance can be obtained as:

$$R = \frac{1}{2} \left(\frac{\phi - \phi_0}{2\pi} \right) \lambda \quad . \tag{3}$$

According to the above equation, in actual tests, as long as the microwave operating frequency is selected and the initial phase of the reference signal and the wavelength are known, the phase difference between the echo signal and the reference signal can be collected and calculated by the hardware circuit, and then the measurement distance R can be obtained[17-19].

In this study, the operating frequency point of the microwave sensor is selected near 24 GHz. This frequency point is selected by comprehensively considering the actual blade tip clearance range of aeroengines, the expected accuracy requirements for blade tip clearance measurement, and the feasibility of actual high-frequency circuit design, ensuring the feasibility of the microwave sensor test.
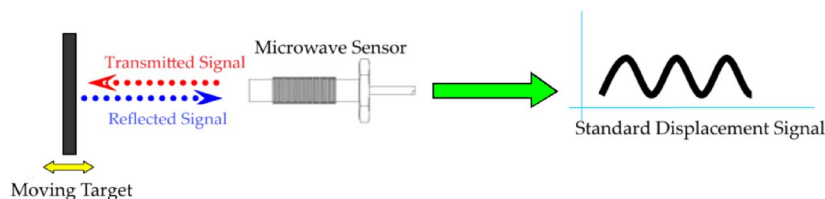

Fig. 1. Schematic diagram of the microwave sensor measurement principle.

Dynamic measurement theory for high-speed blades

For high-speed rotating blades (350–450 m/s), the Doppler effect induces a frequency shift Δf in the reflected microwave signal, expressed as:

$$\Delta f = \frac{2v}{\lambda} \cos \theta \# (4) \quad .$$

(4)

where v is the blade tip velocity, λ is the microwave wavelength, and θ is the angle between the blade motion direction and the sensor's radiation axis. For the 24 GHz sensor ($\lambda \approx 12.5$mm) and $v = 400$ m/s at $\theta = 0°$, the frequence shift is $\Delta f = 64$ kHz. This shift introduces a phase error $\Delta\phi$ in the measurement:

$$\Delta\phi = 2\pi\Delta f \Delta T \quad .$$

(5)

Where T is the signal sampling period. For a sampling frequency of 100 MHz (T = 10 ns), leading to a phase error $\Delta\phi \approx 0.04°$, equivalent to a clearance error of 0.0014 mm. This error is negligible compared to the sensor's resolution.

Structural design of the microwave sensor

The key component of the microwave sensor is the probe antenna, which is responsible for efficiently radiating microwave signals toward the blade tip and receiving the echo signals reflected by the tip end face. When the microwave sensor is used for tip clearance testing, the probe antenna is installed in an opening of the engine casing, imposing special requirements on the design of the probe antenna due to its unique working mode and environment. These requirements mainly include: (1) The probe should preferably have a cylindrical shape for easy installation; (2) The outer diameter of the probe should be minimized; (3) The probe structure must be stable and high-temperature resistant. Considering these factors and analyzing the measurement principle of tip clearance based on the microwave phase method, a microwave sensor probe antenna with a resonant cavity structure is designed, as shown in the schematic diagram of Fig. 2. Its structure consists of a cylindrical resonant cavity formed by a metal-made sensor casing. One end of the resonant cavity is short circuited by a metal wall, and the other end is open for radiating microwave signals outward. The coaxial cable feeds the resonant cavity at the short-circuited end, penetrates the short-circuited wall, extends into the resonant cavity, and combines with the coupling mechanism to achieve the mutual transmission of microwave signals between the coaxial cable and the resonant cavity[20]. To improve the sensor's environmental adaptability during the blade tip clearance test of aeroengines and protect the internal coupling structure of the sensor from the high-temperature combustibles and pollutants of the engine, a ceramic window is added at the open port of the resonant cavity to increase the sensor's high-temperature resistance.

To improve the sensor's structural stability and coupling degree, a stepped coupling structure is adopted. The specific coupling structure is shown in Fig. 3. A three-layer stepped structure is designed, with each step width being the same as that of the inner conductor of the cable and the top of the first-layer step connected to the inner conductor of the cable. The specific shape and size of the coupling structure determine the sensor's specific operating frequency.

Modeling and calculation of the microwave sensor

Referring to the sensor structure shown in Fig. 2, the three-dimensional electromagnetic field calculation software CST-MWS is employed to model the microwave sensor with a resonant cavity structure. Consequently, the specific dimensions of the sensor–probe antenna must be determined via computer modeling and optimized model calculations. The size and structure of the coupling structure determine the degree of coupling of the microwave signal transferred from the coaxial cable to the resonant cavity. Thus, adjusting and optimizing the calculation of its size in the model is essential to ensure that the amplitude of the reflection coefficient at the sensor port exhibits a very low peak near 24 GHz. When operating at this peak point, the reflected microwave signal within the sensor is minimized, and most of the energy can be radiated outward through the sensor.

Figure 4 shows the calculation model diagram of the microwave sensor with a resonant cavity structure. The ceramic window has a thickness of 2.1 mm, a dielectric constant of 8.4, and the sensor probe has an outer
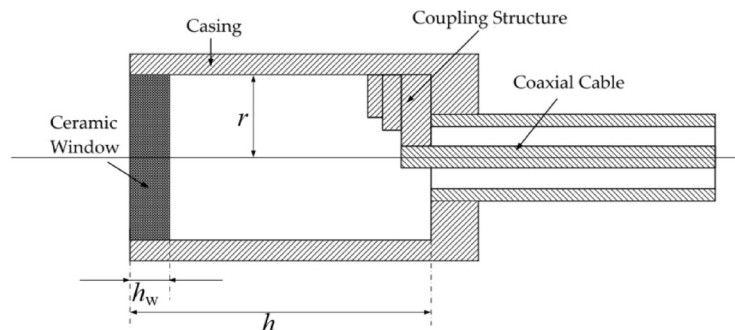

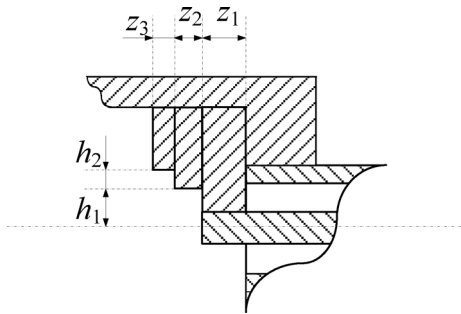**Fig. 2.** Structural diagram of the microwave sensor with a resonant cavity structure.

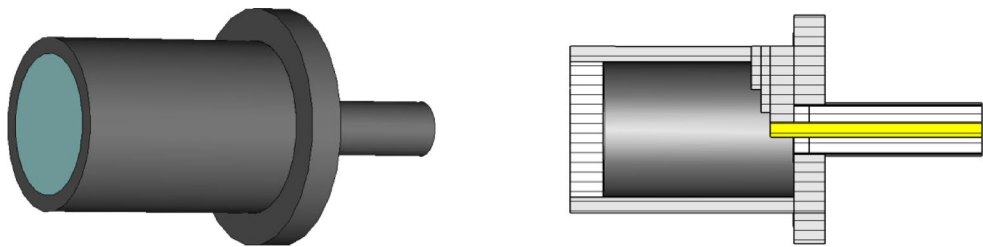**Fig. 3**. Schematic diagram of the sensor coupling structure.

Fig. 4. Calculation model of the microwave sensor with a resonant cavity structure.

Parameter	Dimension (mm)	Remarks
r	4.26	Overall radius of the probe antenna
h_w	2.1	Thickness of the dielectric window
h	14.13	Length of the resonant cavity
z_1	1.5	Axial length of the first-step in the coupling structure
z_2	0.6	Axial length of the second-step in the coupling structure
z_3	0.67	Axial length of the third-step in the coupling structure
h_1	0.3	Radial length of the second-step in the coupling structure
h_2	0.9	Radial length of the third-step in the coupling structure

Table 1. Structural dimension parameters of the sensor probe antenna.

diameter of 10.7 mm. The internal structural dimensions of the sensor obtained through final optimization calculations are listed in Table 1.

Figure 5 shows the amplitude–frequency curve of the reflection coefficient at the sensor port obtained through calculation. The lowest peak point of the curve lies at 23.973 GHz on the abscissa, and the amplitude of the reflection coefficient at this point is 0.01, demonstrating that this resonant cavity structured sensor possesses excellent microwave transmission performance. At this operating frequency, most of the energy emitted by the signal source is radiated outward through the probe, which is conducive to accurate monitoring of the blade tip clearance.

Figure 6 shows the electric field and energy distribution diagrams inside the resonant cavity of the sensor at an operating frequency of 23.973 GHz. The microwave signal transmitted in the coaxial cable can be smoothly coupled into the cylindrical resonant cavity via the stepped feeding structure, exciting a strong electric field in the resonant cavity. As seen from the energy distribution diagram, most of the energy in the resonant cavity can be radiated outward through the probe port, with the radiation direction along the axial direction forward, facing the engine blade, enabling the transmitted signal to be smoothly reflected to the sensor antenna by the blade tip.

Figure 7 shows the 3D and 2D radiation patterns of the microwave sensor probe antenna at the operating frequency. The sensor antenna has a maximum radiation gain of 10.06 dB, a radiation efficiency of 97%, and the maximum radiation direction of the antenna is 0°, namely, along the positive z-axis direction, which is precisely the direction where the sensor probe faces the blade tip. The 3 dB radiation angle is 39.7°. Clearly, this microwave sensor antenna features a large radiation gain, high radiation efficiency, and small radiation angle, demonstrating its ability to effectively concentrate and transmit microwave signals toward the blade tip end face, which is beneficial for measuring the blade tip clearance of engine blades. The resonant cavity structure is optimized for high-speed applications, with a narrow radiation angle (39.7°) to minimize the exposure time of
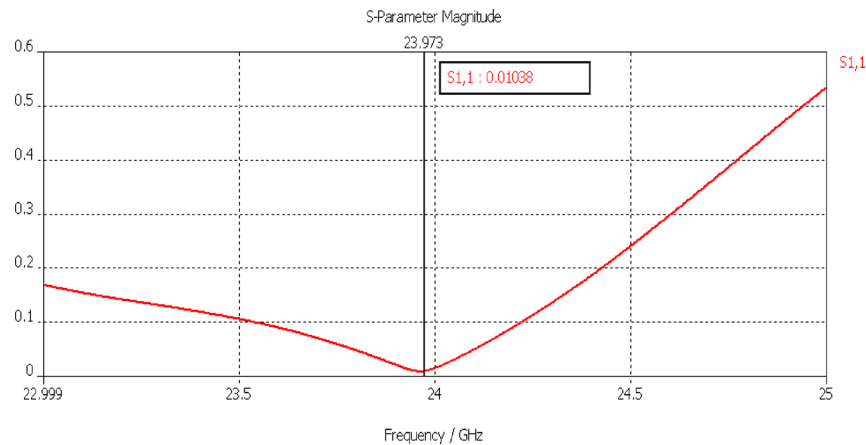
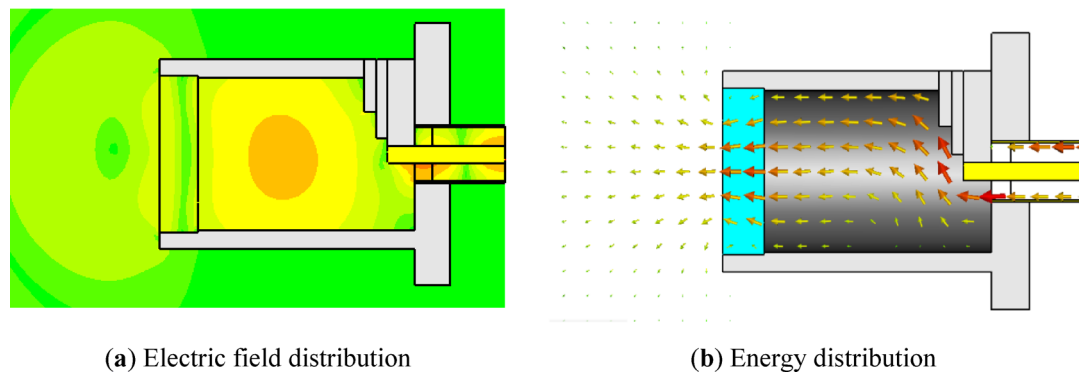**Fig. 5**. Amplitude–frequency curve of the reflection coefficient at the port of the microwave sensor.

(**a**) Electric field distribution

(**b**) Energy distribution

Fig. 6. Electric field and energy distribution diagrams inside the microwave sensor at theoperating frequency point.

(**a**) 3D Radiation pattern
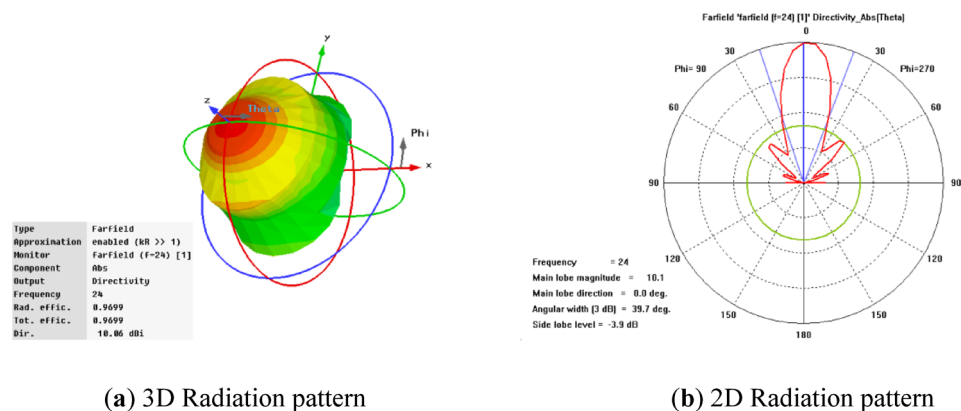
(**b**) 2D Radiation pattern

Fig. 7. 3D and 2D radiation patterns of the microwave sensor probe antenna.

each blade tip. The stepped coupling structure enhances signal fidelity, reducing transient distortion caused by rapid blade passage.

The processed components and the overall prototype of the microwave sensor with a resonant cavity structure are depicted in Fig. 8.

Design and implementation of the high-temperature resistant microwave probe

When a microwave sensor is used to test the blade tip clearance of an engine, the sensor probe is installed at the opening of the engine casing, and the end face of the sensor probe directly faces the high-temperature gas in the engine. Thus, ensuring the high-temperature resistance of a microwave sensor is a key technology that needs to be addressed in sensor design. First, starting from the processing materials and structure of the sensor, suitable high-temperature resistant materials and sensor structures are selected to ensure the overall structural stability of the sensor probe in a high-temperature environment. Second, simulation calculations and analyses are conducted to evaluate the impact of changes in material parameters at high temperatures on sensor performance and ensure good blade tip clearance test performance at high temperatures.

Selection of high-temperature resistant materials

To ensure the structural stability of a microwave sensor under high-temperature conditions, it is essential to select appropriate high-temperature resistant metal and dielectric materials for processing. The subsequent content analyzes the materials of each component on the basis of the characteristics of the microwave sensor with a resonant cavity structure. Since the sensor casing is installed in the engine casing, the selection of the sensor casing material needs to consider the thermal matching between the sensor and the engine casing simultaneously. Thus, the nickel-based alloy GH4169, which is identical to the engine casing material, is employed as the casing material. The sensor's insulating dielectric window must be high-temperature resistant and capable of withstanding the high-pressure environment in the engine to safeguard the internal structure of the sensor from damage. A dense silicon nitride ceramic sheet is utilized. This material exhibits excellent high-temperature stability. By measuring its dielectric constant in the high-frequency band at high temperatures, its dielectric constant was 8.4. The microwave transmission cables also need to be high-temperature resistant. To minimize the transmission loss of microwaves in the cable, the dielectric constant of the high-temperature resistant insulating material should be as small as possible. The inner and outer conductors and insulating dielectric material of the employed coaxial cable are oxygen-free copper and foamed silica, respectively. Foamed silica has a dielectric constant of only 1.9 and can withstand temperatures of up to thousands of degrees Celsius. The outermost layer of the cable is nickel-plated or covered with a stainless-steel sheath to protect the cable and prevent copper oxidation. The basic properties of the high-temperature resistant materials utilized for each component of the microwave sensor are summarized in Table 2. When comprehensively considering the material selection of each component of the sensor, the sensor materials meet high-temperature requirements in terms of thermal stability and structural integrity.

Simulation calculation of the high-temperature resistance performance of the sensor

The high-temperature environment in the engine has two main impacts on the performance of the microwave sensor. First, thermal expansion causes the internal structure size of the sensor to increase. Owing to the significant difference in the expansion coefficients of metal and nonmetal components, gaps resulting from the different expansion sizes of components made of different materials easily occur. The other is that the increase in ambient temperature leads to changes in the material characteristic parameter values, such as the dielectric constant value of the ceramic medium inside the sensor, thereby altering the microwave signal transmission performance. Regarding the first impact, given that the size of the sensor probe itself is very small, the thermal expansion size at high temperatures is even smaller. Through simulation calculations, it has been found that its impact on sensor performance is not obvious. To quantitatively validate this, we calculated the thermal expansion effects of key components at 1000 °C. The casing (GH4169, thermal expansion coefficient $\alpha \approx 13 \times 10^{-6}$/°C) with an initial outer diameter of 10.7 mm expands radially by approximately $\Delta D = \alpha \cdot \Delta T \cdot D = 13 \times 10^{-6} \times 1000 \times 10.7 \approx 0.14$ mm. The ceramic window (Si_3N_4, $\alpha \approx 3.2 \times 10^{-6}$/°C) of thickness 2.1 mm expands axially by $\Delta L \approx 0.007$ mm. Such dimensional changes alter the resonant cavity volume by < 0.3%, inducing a frequency shift of < 12 MHz (from CST simulations), which is negligible compared to the 330 MHz shift caused by dielectric constant changes (Fig. 9a). Consequently, the main reason for the change in the performance of the microwave sensor at high temperatures is the impact caused by the change in the dielectric constant of its internal ceramic medium.

In the stepped coupling resonant cavity microwave sensor, there are three dielectric components. The first is the dielectric window at the front end of the probe, which is composed of a dense silicon nitride material with a dielectric constant of approximately 8.4 at room temperature. The second is the ceramic retaining ring at the cable port, which is used to seal the dielectric powder and is made of quartz ceramic material with a dielectric constant of approximately 3.15 at room temperature. The third is the powdery foamed silica medium inside the coaxial cable, which has a dielectric constant of 1.9 at room temperature. By measuring the dielectric constants

Component	Requirements	Material	Melting Point/°C	Characteristics	Oxidation Resistance
Casing	High-temperature resistance, matching with the engine casing	Nickel-based GH4169	1260 ~ 1320	/	Good
Dielectric window	High-temperature resistance, dense, high-temperature stability	Silicon nitride ceramic	2000	$\varepsilon = 8.4$	Good
Inner and outer conductors of the cable	High-temperature resistance, high conductivity	Oxygen-free copper	1083	$\rho = 16.78$	Poor
Inner transmission medium of the cable	High-temperature resistance, low dielectric constant	Foamed silica	1670	$\varepsilon = 1.9$	Good

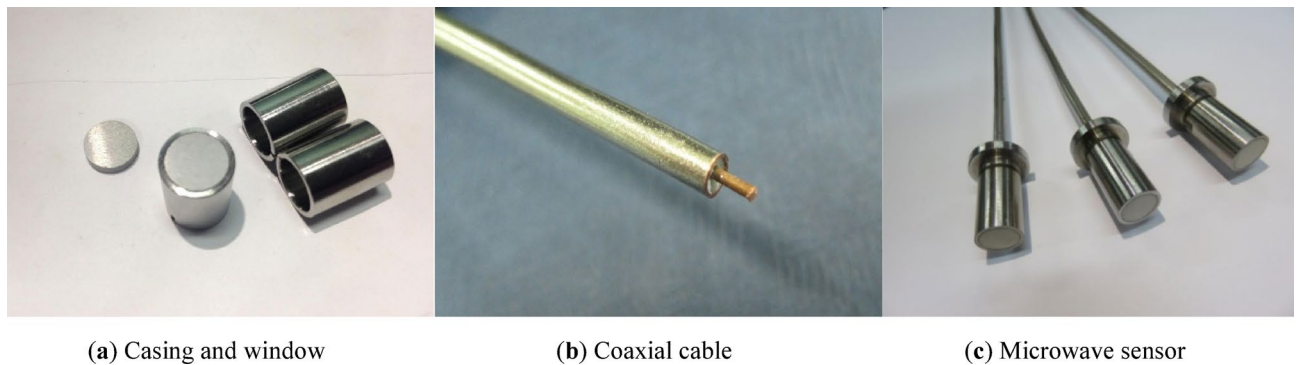**Table 2.** Basic properties of the materials for each component of the sensor.

(**a**) Casing and window   (**b**) Coaxial cable   (**c**) Microwave sensor

Fig. 8. Photos of the microwave sensor

(**a**) Resonant frequency shift   (**b**) Reflection coefficient amplitude
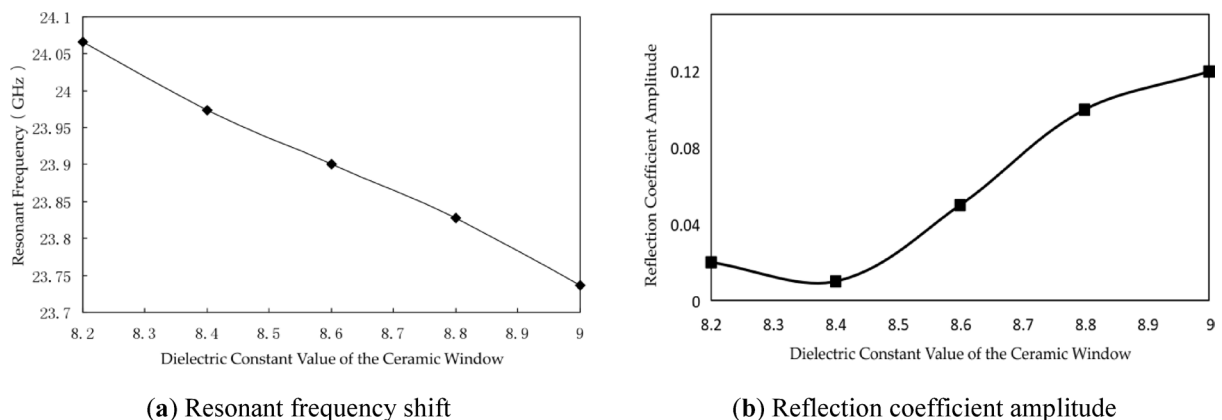
Fig. 9. Influence of the change in the dielectric constant of the ceramic window on the sensor performance.

of materials at high temperatures, it is known that as the ambient temperature gradually increases, the dielectric constants of high-frequency dielectrics gradually increase. Owing to the different high-temperature dielectric properties of different materials, the degrees of change vary. As the ambient temperature increases from room temperature to 1000 °C, the dielectric constants of different dielectrics increase to varying degrees. Specifically, the increase in the dielectric constant of dense silicon nitride is approximately 10% of its original value, whereas that of the quartz ceramic material is approximately 2% of its original value. On this basis, in the calculation model, the dielectric constants of different dielectrics are altered to calculate the changes in sensor performance.

Figures 9 and 10, respectively illustrate the changes in the sensor's resonant frequency and the amplitude of the reflection coefficient at the original operating frequency point (23.973 GHz) when the two dielectrics are in the microwave sensor, namely, the ceramic window and the ceramic retaining ring. In terms of high-temperature resistance performance, simulation calculations focused on studying the impact of changes in the dielectric constant of the internal ceramic media of the sensor in a high-temperature environment on its performance. The sensor contains multiple dielectric components, such as a dense silicon nitride dielectric window at the front end of the probe, a quartz ceramic retaining ring at the cable port, and a foamed silica medium inside the coaxial cable.

A change in the dielectric constant has a significant effect on sensor performance. Taking the ceramic window as an example, when the dielectric constant increases from 8.2 to 9, the resonant frequency of the sensor decreases monotonically, with a decrease of approximately 330 MHz, and the amplitude of the reflection coefficient at the operating frequency point increases monotonically, reaching 0.12. This indicates that the energy attenuation inside the sensor increases at high temperatures. However, at this time, the energy of the reflected signal accounts for only 1.4% of the transmitted signal energy, and most of the microwave signals can still be transmitted normally, allowing the sensor to maintain normal operation.

In contrast, the change in the dielectric constant of the ceramic retaining ring has a comparatively minor effect on the sensor performance. When the dielectric constant increases from 3.1 to 3.2, the change range of the resonant frequency is only 20 MHz, and the maximum amplitude of the reflection coefficient at the operating frequency point is approximately 0.018. This is mainly because the dielectric constant of the ceramic retaining ring material is closer to that of the coaxial cable transmission medium, and its size is much smaller than that of the dielectric window. Additionally, the installation position of the ceramic retaining ring is less heated. These results provide important evidence for evaluating the reliability of sensors in high-temperature environments and offer directions for further optimizing sensor design.
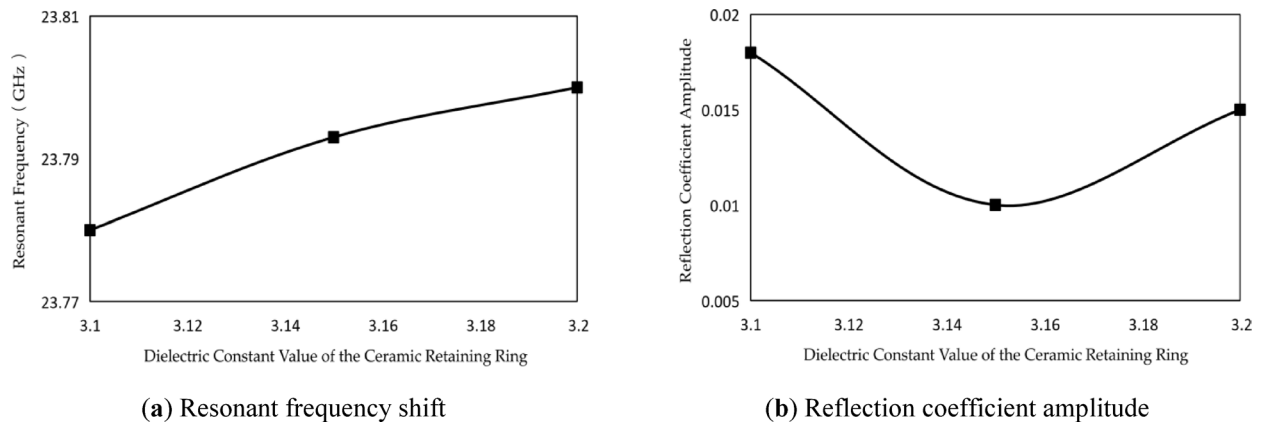
(**a**) Resonant frequency shift   (**b**) Reflection coefficient amplitude

Fig. 10. Influence of the change in the dielectric constant of the ceramic retaining ring on the sensor performance.
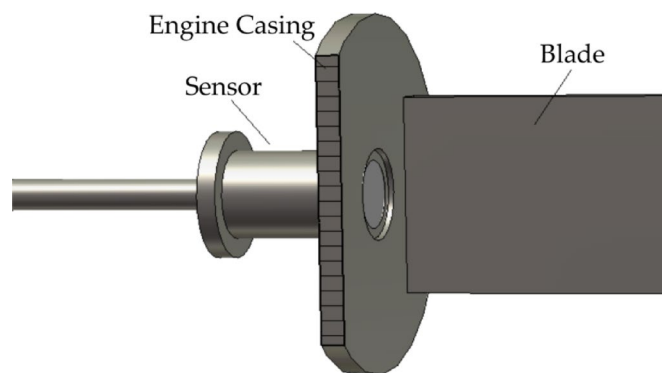

Fig. 11. Calculation model for simulating blade tip clearance measurements.

Simulation calculation of the microwave sensor for blade tip clearance distance measurement

Figure 11 depicts the calculation model established for simulating the blade tip clearance test of the engine via this structured microwave sensor. In the model, the sensor probe is retracted in the simulated engine casing, and the distance between the front face of the probe and the inner wall of the engine casing is 0.5 mm. To simplify the calculation model, the tip end face of the simulated blade is set to be rectangular with dimensions of 3 mm30 mm. Since the microwave radiation direction of the sensor probe is linearly polarized, when the sensor is installed, the long side direction of the tip end face of the measured blade must be consistent with the polarization direction of the probe to ensure that the transmitted microwave signal can be reflected by the tip end face to the greatest extent. In the calculation model, the standard blade tip clearance value is adjusted by changing the distance between the tip end face and the inner wall of the simulated engine casing.

Figures 12 and 13, respectively illustrate the change curves of the sensor's test phase and test distance values when the standard clearance obtained from the sensor simulation calculation varies within the range of 0–6 mm. A clear correlation exists between the sensor's measured phase value and the clearance distance. Specifically, as the clearance distance increases, the measured phase value gradually decreases. This trend is highly consistent with the theoretical analysis, indicating the correctness and stability of the sensor's measurement principle. Moreover, when the measured phase value is substituted into the equation, the calculated true measured value gradually increases. When the standard clearance increases from 0 to 6 mm, the measured phase decreases by approximately 316°, and the true measured value increases by 5.49 mm. This demonstrates that the sensor has excellent measurement resolution and can precisely capture subtle changes in blade tip clearance.

Figure 14 shows a comparison of the sensor test phase curves with retraction values of 0.1 mm, 0.5 mm, and 0.8 mm in the engine casing wall. Evidently, the change trends of the test phase curves were basically consistent. However, as the retraction value increased, the curves shifted downward. This is because an increase in the retraction value leads to a corresponding increase in the distance between the sensor probe port and the actual blade tip, resulting in a decrease in the phase value corresponding to the initial value. Notably, although different retraction values affect the initial phase of the measurement, all the test curves can meet the requirements for blade tip clearance measurement. Nevertheless, for each determined retraction value, a corresponding calibration curve needs to be obtained anew to ensure the accuracy of the measurement results. This characteristic is crucial in practical applications. Since the installation positions of sensors on the engine casing may vary, understanding
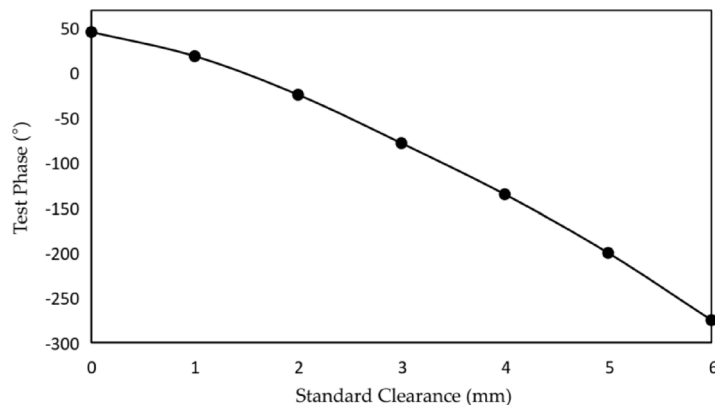
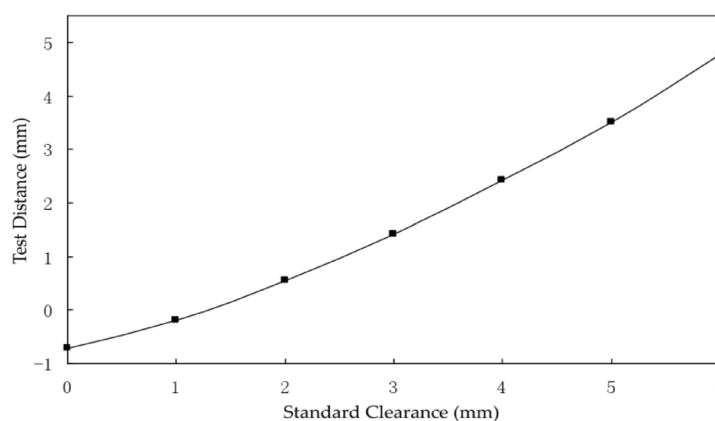**Fig. 12**. Curve of the microwave sensor test phase changing with the clearance.

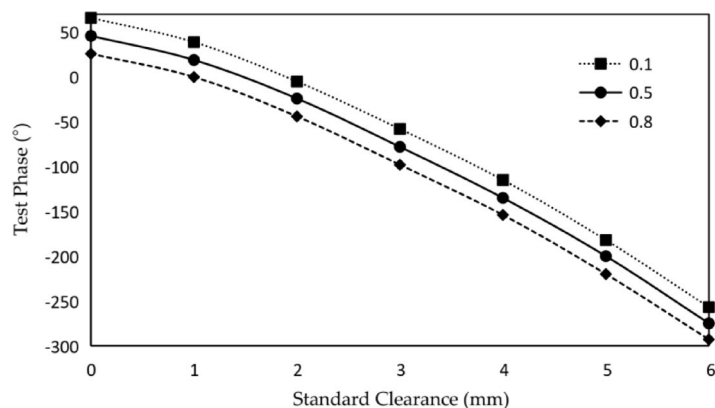**Fig. 13**. Curve of the microwave sensor test distance changing with the clearance.

Fig. 14. Test curves of the microwave sensor with different retraction distances.

the measurement characteristics at different retraction distances is helpful for optimizing the installation and calibration processes of the sensors.

Dynamic test under high-speed rotation

A schematic diagram of the dynamic performance test bench for the microwave sensor is shown in Fig. 15. The simulation disk equipped with simulated blades is mounted on a motor with controllable rotational speed. The simulation disk is uniformly distributed with 20 blades, each featuring identical shape and dimensions, and the blade tip is rectangular with an end-face size of 3 mm×30 mm. The sensor probe is installed in a hole of the
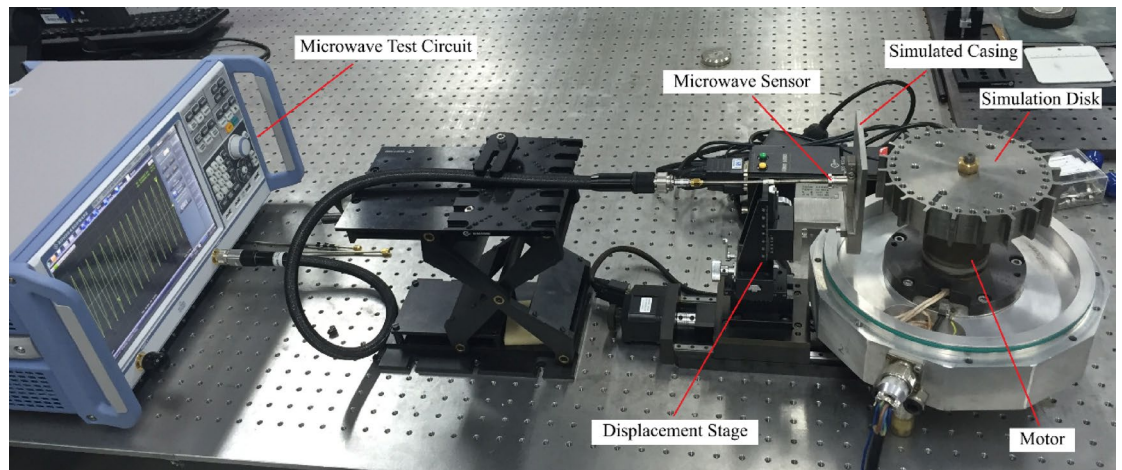
Fig. 15. Schematic of the dynamic performance test bench for the microwave sensor.
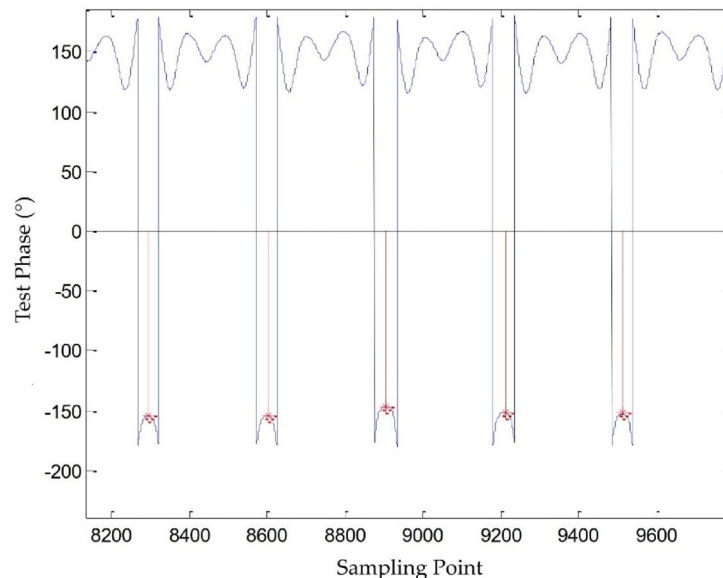

Fig. 16. Local blade dynamic test results at 0.5 mm clearance.

simulated casing. The displacement stage has a three-dimensional structure, enabling fine adjustment of the sensor position and providing the standard tip clearance. The other end of the microwave sensor is connected to the microwave test circuit via a coaxial cable. The test circuit includes a microwave signal source and a demodulation circuit for processing the sensor's reflected signals.

During the entire clearance measurement process, as the sensor operates in a continuous-wave mode, it measures and collects signals at various positions of the disk. An effective algorithm must be employed to extract the measurement values at the blade tip positions from the continuously collected signals at different positions. In the analysis, the measured microwave signals are first converted into digital signals, followed by transformation using the Fast Fourier Transform (FFT) method. The measurement signals are decomposed into different velocity components based on the blade's motion direction relative to the sensor end-face (decomposable into velocity components where the blade moves toward and away from the sensor). The Inverse Fast Fourier Transform (IFFT) is then used to convert the frequency-domain signals into time-domain signals. The amplitude component of the complex time-domain signal represents the magnitude of the reflected energy received by the sensor, while the phase component represents the distance to the sensor. By comparing the measured amplitude component with a preset threshold, it can be determined whether a blade passes through the sensor. The blade tip position is identified using the zero-velocity point (where the phases of the components moving toward and away from the sensor are equal) within the blade region.

The following Fig. 16 presents the dynamic test phase diagram at a 0.5 mm clearance position under 1000 rpm. Figure 17 shows the microwave sensor clearance test curve obtained through experiments at 1000 rpm. Notably, within the standard clearance range of 0.5–5 mm, the curve is smooth and monotonically increasing, consistent
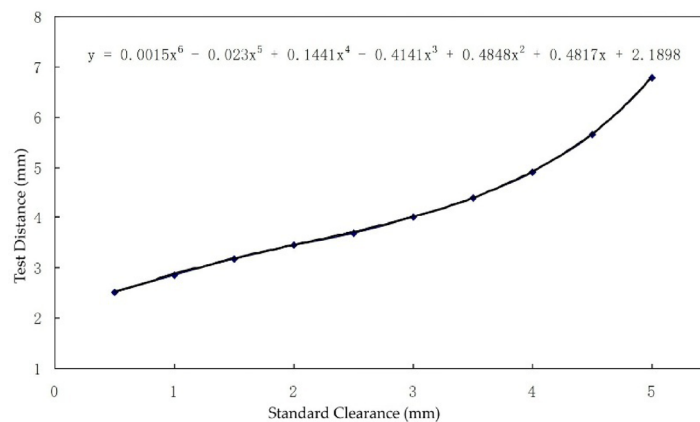
$$y = 0.0015x^6 - 0.023x^5 + 0.1441x^4 - 0.4141x^3 + 0.4848x^2 + 0.4817x + 2.1898$$

Fig. 17. Dynamic test curve of the microwave sensor at 1000 rpm.

with theoretical analysis. At small clearance positions, the curve has a lower slope, while at large clearance positions, the slope increases, adhering to the principles of the near-field and radiation near-field induction of the sensor probe antenna.

Discussion

Compared with existing technologies, the high-temperature resistant microwave blade tip clearance sensor designed in this study exhibits significantly better measurement performance in high temperature environments. From the perspective of the measurement principle, the use of the microwave phase method to obtain the real-time change in the blade tip clearance via the phase difference between the reflected signal and the reference signal presents unique advantages over traditional measurement technologies. Compared with capacitive measurement technologies, this sensor is immune to environmental humidity, oil, and other factors and demonstrates greater measurement stability. Compared with inductive measurement technologies, it has a lower reliance on the electromagnetic characteristics of the measured object and a broader application range. Compared with optical measurement technologies, in the complex environment inside the engine, microwave transmission is less influenced by oil, smoke, etc., and the measurement reliability is markedly enhanced. In the actual test simulation, the sensor features a smooth measurement phase and measurement distance change curves within the 0–6 mm standard clearance range, with good measurement resolution. This enables accurate reflection of the changes in the blade tip clearance and offers robust monitoring support for the efficient and stable operation of aeroengines.

In terms of high-temperature resistance performance, this study ensures the structural stability of the sensor in a high-temperature environment through meticulous selection of high-temperature-resistant materials. For example, nickel-based alloy GH4169 is employed as the casing material, dense silicon−nitride ceramic sheets are used as the dielectric window, and oxygen-free copper and foamed silica are utilized for the microwave transmission cable. Furthermore, while thermal expansion of materials is inevitable at high temperatures, calculations confirm its minimal impact on measurement accuracy. The maximal radial expansion of the sensor casing (0.14 mm at 1000 ℃) translates to a blade tip clearance measurement error of < 0.05 mm (via Eq. 3). This error is an order of magnitude smaller than the sensor's typical resolution, demonstrating that the selected materials (GH4169/Si_3N_4) effectively suppress measurement errors induced by structural distortion. Simulation calculations indicate that despite high temperatures causing changes in the dielectric constant of ceramic media, the sensor can still function normally. Unlike traditional proximity sensors, this microwave sensor maintains accuracy at high speeds due to the phase-based measurement principle mitigates Doppler errors, as validated by dynamic test. This achievement holds significant application value in the measurement of blade tip clearance in the high-temperature environment of aeroengines, resolving the issue of insufficient high-temperature resistance performance of existing sensors and enabling gap monitoring during the long-term stable operation of engines.

Nonetheless, this study also has certain limitations. First, the simulation calculation does not comprehensively consider the impact of complex working conditions, such as dynamic airflow and vibration inside the engine, on the measurement. Second, the long-term high-temperature stability and thermal cycling fatigue effects of materials have not been experimentally verified. Future research can integrate actual engine bench tests to further increase the robustness of the sensor in dynamic environments and explore adaptive compensation algorithms to address dielectric constant drift under extreme temperatures. Moreover, the sensor design can be expanded to other frequency bands or structural forms to meet the gap measurement requirements of different aircraft engines.

Overall, the design scheme of a high-temperature resistant microwave sensor based on the resonant cavity principle proposed in this study offers new ideas and methods for addressing the issue of accurate measurement of aeroengine blade tip clearance. Its potential application value extends beyond the aeroengine field. It also has extensive application prospects in other industrial scenarios involving gap measurement in high-temperature environments, such as gap monitoring of high-temperature industrial equipment, such as gas turbines and

nuclear reactors. This is expected to drive technological development and equipment performance improvement in related fields.

Conclusion

This study designed a high-temperature resistant microwave blade tip clearance sensor on the basis of the resonant cavity principle. By optimizing the resonant cavity structure, selecting high-temperature resistant materials (Si_3N_4 ceramics, GH4169 alloy), and conducting a coupling design, high-precision measurement of the blade tip clearance in a 1000 °C environment was accomplished. Thermal expansion of materials contributes negligibly to measurement error, further ensuring reliability in extreme thermal environments. The sensor exhibits a radiation efficiency of 97% at the 24 GHz frequency point, a reflection coefficient as low as 0.01, and the impact of dielectric constant changes on its performance is manageable, which is significantly superior to that of traditional capacitive and optical sensors. The sensor's capability to function in dynamic operational environments facilitates its seamless integration into engine Prognostics and Health Management (PHM) systems, thereby enhancing the reliability of real-time health monitoring frameworks. In the future, more emphasis can be placed on dynamic environment verification, long-term material stability testing, and the development of multifrequency band sensors to broaden their application scope in aerospace and energy-related equipment.

Data availability

Data sets generated during the current study are available from the corresponding author on reasonable request.

References

1. Peng, H., Gao, F., Tian, S. & Yang, X. A microwave sensor for monitoring and measuring the blade tip clearance of aero-engine. In *Proceedings of the 2024 International Conference on Microwave and Millimeter Wave Technology (ICMMT)*, 1–3. (2024). https://doi.org/10.1109/ICMMT61774.2024.10671827
2. Yu, B., Ke, H., Shen, E. & Zhang, T. A review of blade tip clearance-measuring technologies for gas turbine engines. *Meas. Control.* **53**, 339–357. https://doi.org/10.1177/0020294019877514 (2020).
3. Aslinezhad, M. & Hejazi, M. A. Turbine blade tip clearance determination using microwave measurement and k-nearest neighbour classifier. *Measurement* **151**, 107142. https://doi.org/10.1016/j.measurement.2019.107142 (2020).
4. Guo, X., Liu, H. & Zhou, Z. Improving the blade tip clearance measurement method based on blade tip timing: accounting for rotor speed variations and non-uniform blade-by-blade tip clearance. *Measurement* **242**, 115777. https://doi.org/10.1016/j.measurement.2024.115777 (2025).
5. Stubbs, J. D. & Shahid, M. A. Blade tip clearance measurement systems for high speed turbomachinery applications and the potential for blade tip timing applications. In *Proceedings of the ASME Turbo Expo 2020: Turbomachinery Technical Conference and Exposition*, V008T20A021. (2020). https://doi.org/10.1115/GT2020-15403
6. Fernández, R., Amorebieta, J., Durana, G., Beloki, J. & Zubia, J. Performance comparison among three optical fibre-based displacement sensors for blade tip clearance measurements. In *Proceedings of the 2018 5th IEEE International Workshop on Metrology for Aerospace (MetroAeroSpace)*, 657–662. (2018). https://doi.org/10.1109/MetroAeroSpace.2018.8453515
7. Li, H., Wu, S., Yang, Z., Yan, R. & Chen, X. Measurement methodology: blade tip timing: A non-contact blade vibration measurement method. *IEEE Instrum. Meas. Mag.* **26**, 12–20. https://doi.org/10.1109/MIM.2023.10328672 (2023).
8. Li, H., Tian, S. & Yang, Z. A novel blade vibration monitoring experimental system based on blade tip sensing. *Materials* **15**, 6987. https://doi.org/10.3390/ma15196987 (2022).
9. Cao, J. et al. Simultaneous measurement for blade tip clearance and vibration based on capacitive probe. In *Proceedings of the 2023 International Conference on Sensing, Measurement & Data Analytics in the Era of Artificial Intelligence (ICSMD)*, 1–6. (2023). https://doi.org/10.1109/ICSMD60522.2023.10490558
10. Li, H. et al. Adaptive iterative approach for efficient signal processing of blade tip timing. *IEEE Trans. Instrum. Meas.* **70**, 1–13. https://doi.org/10.1109/TIM.2021.3107588 (2021).
11. Li, W. et al. Simultaneous measurement of blade tip clearance and blade tip timing with microwave sensor. *IEEE Trans. Instrum. Meas.* **73**, 1–12. https://doi.org/10.1109/TIM.2024.3375413 (2024).
12. Cao, J. et al. Biprobes blade tip timing method for frequency identification based on active aliasing time-delay Estimation and dealiasing. *IEEE Trans. Ind. Electron.* **70**, 1939–1948. https://doi.org/10.1109/TIE.2022.3165252 (2023).
13. Zhou, L., He, C., Cao, J., Yang, Z. & Chen, X. Frequency identification method based on active aliasing of biprobes blade tip timing without once-per-revolution. *Measurement* **242**, 115868. https://doi.org/10.1016/j.measurement.2024.115868 (2025).
14. Gil-García, J. M., García, I., Zubia, J. & Aranguren, G. Blade tip clearance and time of arrival immediate measurement method using an optic probe. In *Proceedings of the 2015 IEEE Metrology for Aerospace (MetroAeroSpace)*, 118–122. (2015). https://doi.org/10.1109/MetroAeroSpace.2015.7180638
15. Violetti, M., Skrivervik, A. K., Xu, Q. & Hafner, M. New microwave sensing system for blade tip clearance measurement in gas turbines. In *Proceedings of the IEEE SENSORS*, 1–4. (2012). https://doi.org/10.1109/ICSENS.2012.6411229
16. JDMD Editorial Office. et al et al. New sensing technologies for monitoring machinery structures and manufacturing processes. *J. Dyn. Monit. Diag.* **2**, 69–88. https://doi.org/10.37965/jdmd.2023.322 (2023).
17. Niu, G., Duan, F., Liu, Z., Jiang, J. & Fu, X. A high-accuracy non-contact online measurement method of the rotor-stator axial gap based on the microwave heterodyne structure. *Mech. Syst. Signal. Process.* **150**, 107320. https://doi.org/10.1016/j.ymssp.2020.107320 (2021).
18. Wang, Z. et al. An OPR-free blade tip timing method for rotating blade condition monitoring. *IEEE Trans. Instrum. Meas.* **70**, 1–11. https://doi.org/10.1109/TIM.2020.3033732 (2021).
19. Zhang, J., Duan, F., Niu, G., Jiang, J. & Li, J. A blade tip timing method based on a microwave sensor. *Sensors* **17**, 1097. https://doi.org/10.3390/s17051097 (2017).
20. Zhu, C., Gerald, R. E., Chen, Y. & Huang, J. Probing the theoretical ultimate limit of coaxial cable sensing: measuring nanometer-scale displacements. *IEEE Trans. Microw. Theory Tech.* **68**, 816–823. https://doi.org/10.1109/TMTT.2019.2951099 (2020).

Author contributions

The paper was authored by H.S.

Funding

Declarations

Competing interests

The authors declare no competing interests.

Additional information

Correspondence and requests for materials should be addressed to H.S.

Reprints and permissions information is available at www.nature.com/reprints.

Publisher's note Springer Nature remains neutral with regard to jurisdictional claims in published maps and institutional affiliations.